

1 Sea ice melt drives vertical pCO₂ variability modulating 2 air-sea gas exchange

3
4 Henry C. Henson^{1,2}, Dorte H. Søgaard^{2,3,7}, Bjarne Jensen⁶, Kunuk Lennert⁴, Tim
5 Papakyriakou⁵, Mikael K. Sejr^{1,2}, Jakob Sievers⁶, Søren Rysgaard^{2,7}, and Lise Lotte
6 Sørensen^{2,6}

7
8 ¹Department of Ecoscience, Aarhus University, Aarhus, 8000, Denmark

9 ²Arctic Research Center, Aarhus University, Aarhus, 8000, Denmark

10 ³Greenland Climate Research Cluster, Greenland Institute of Natural Resources, Nuuk, 3900, Greenland

11 ⁴UiT, The Arctic University of Norway, Tromsø, 9037, Norway

12 ⁵Centre for Earth Observation Science, University of Manitoba, Winnipeg, MB, R3T 2N2, Canada

13 ⁶Department of Environmental science, Aarhus University, Roskilde, 4000, Denmark

14 ⁷Department of Biology, Center for Ice-free Arctic Research, Aarhus University, Aarhus, 8000, Denmark

15
16 Corresponding author: Henry C. Henson (hch@ecos.au.dk)

17 18 19 20 21 22 **Key Points:**

- 23 • Spring melting of sea ice and snow introduces distinct heterogeneity in surface water
24 conditions within coastal Arctic oceans.
 - 25 • Standard bulk parameterizations for air-sea CO₂ flux calculations, based on subsurface
26 pCO₂ measurements, may misrepresent flux magnitude during melt periods.
 - 27 • Vertical near-surface CO₂ and temperature gradients must be considered to improve flux
28 estimates in stratified Arctic fjords.
- 29

30 **Abstract**

31 Strong spatial and temporal gradients in salinity, temperature, and carbonate chemistry in Arctic
32 coastal surface waters complicate the estimation of air-sea carbon dioxide (CO₂) exchange,
33 particularly during sea ice breakup. The present study evaluates the applicability of the widely
34 used bulk flux model under such conditions. This approach assumes homogeneous surface
35 conditions and no vertical pCO₂ gradients in the bulk seawater. However, our observations in a
36 stratified Arctic fjord reveal pronounced vertical variability in pCO₂ within the upper water
37 column, including non-linear gradients near the air-sea interface. This results in, widely varying
38 flux estimates depending upon the depth of the pCO₂ measurement used to establish air-sea
39 disequilibrium. Importantly, similarly structured nonlinear pCO₂ profiles were observed across
40 distinct fjord systems and years, suggesting that this vertical heterogeneity may be a
41 characteristic feature of Arctic stratification during sea ice breakup. We recommend
42 incorporating both micrometeorological techniques and high-resolution vertical profiling in
43 Arctic fjords to improve flux estimates of CO₂ in this rapidly changing region.

44 **Plain Language Summary**

45 Sea ice melt adds less-saline water to the surface ocean. This creates vertical gradients in
46 salinity, temperature, and partial pressures of carbon dioxide (pCO₂). The concentration
47 difference of pCO₂ across the air-ocean boundary is used to estimate gas transfer. Thus, the
48 depth that we measure will impact our estimates. Similar patterns were observed in multiple
49 Arctic fjords years apart, suggesting these vertical gradients may be common during the spring
50 melt season.

51 **1 Introduction**

52
53 High latitude coastal oceans are strong sinks for atmospheric carbon dioxide (CO₂), absorbing
54 more CO₂ per unit area than lower latitude regions (Dai et al., 2022; Roobaert et al., 2019). This
55 strong uptake results from both the high solubility of gases in cold water and the intense
56 biological activity typical of these regions. However, climate change is rapidly transforming this
57 carbon sink. The Arctic is warming more than twice as fast as the global average, and sea ice
58 extent has been shrinking by over 13% per decade (Perovich et al., 2020). The loss of sea ice
59 increases CO₂ uptake by exposing larger areas of open water for longer periods, which can
60 further stimulate biological productivity (Arrigo and van Dijken, 2015; Bates and Mathis, 2009;
61 Perovich et al., 2020). However, at the same time, melting sea ice freshens the surface layer and
62 strengthens stratification, limiting vertical mixing with deeper water. Freshwater from melting
63 sea ice and terrestrial run-off creates pronounced gradients in physical properties such as salinity
64 and temperature, as well as chemical properties like dissolved inorganic carbon (DIC) and total
65 alkalinity (TA) (e.g. Henson et al., 2025). As a result, the partial pressure of CO₂ (pCO₂) can
66 vary markedly with depth under melt conditions (Miller et al., 2019).

68

69 This vertical variability in $p\text{CO}_2$ poses a challenge for air-sea CO_2 flux estimation. The transfer
70 of gases between the atmosphere and ocean depends on the difference in concentration between
71 the two as well as the efficiency of the transfer process. Therefore, the bulk flux of CO_2 across
72 the air-sea interface is commonly described as the product of the gas transfer velocity, k (m s^{-1}),
73 CO_2 solubility s ($\text{mol kg}^{-1} \text{atm}^{-1}$), and the partial pressure gradient (μatm) across the air-sea
74 interface (Wanninkhof et al., 2009):

$$F = ks(p\text{CO}_{2_{sea}} - p\text{CO}_{2_{air}}) \quad (1)$$

78 While widely applied, this formulation simplifies a complex process influenced by surfactants on
79 the water surface, bubble-mediated gas exchange, and turbulence (Wanninkhof et al., 2009).
80 Furthermore, surface water heterogeneity, driven by sea ice melt and freshwater runoff from
81 land, complicates the physical and chemical processes governing air-sea CO_2 exchange. As a
82 result, simplified parameterizations commonly used in global carbon flux estimates may be
83 inadequate in these settings.

85 In most studies, $p\text{CO}_2$ is measured several meters below the surface, assuming vertical
86 homogeneity under well-mixed conditions (Jørgensen et al., 2020). However, in stratified waters,
87 where temperature, salinity, and pH can vary with depth, this assumption may lead to substantial
88 errors in flux estimates (Ahmed et al., 2020; Dong et al., 2021; Miller et al., 2019; Watts et al.,
89 2022). In this study, we distinguish between the air-sea interface, the near-surface freshwater
90 lens (approximately the upper 0-0.5 m), and subsurface bulk waters (>1 m depth), as these layers
91 may exhibit substantially different physical and carbonate chemistry conditions during sea ice
92 melt. Previous work in Young Sound demonstrated that snow and sea ice melt can substantially
93 reduce under-ice $p\text{CO}_2$ through dilution and enhanced stratification during the melt season
94 (Verdugo et al., 2025). However, these observations were conducted at a fixed depth below the
95 ice, leaving unresolved how $p\text{CO}_2$ variability evolves vertically during sea ice breakup.

97 Although Arctic surface waters are often undersaturated with respect to atmospheric CO_2 levels
98 and act as CO_2 sinks (e.g. Burgers et al., 2017; Dai et al., 2022; Henson et al., 2024; Laruelle et
99 al., 2014; Roobaert et al., 2019), such assessments typically rely on sparse data collected from
100 0.5-5 m depth during limited periods. Dong et al. (2021) illustrate that high latitude fluxes of
101 CO_2 calculated using the bulk method (based on measurements sampled at 6 m depth) differ
102 significantly from those measured using direct eddy covariance in sea ice melt regions.

104 Gas transfer velocity (k) is often parameterized as a function of wind speed. However, the true
105 driver is mixing in the surface waters, which governs k . Fick's first law of diffusion, which
106 underlies Equation (1), assumes a linear concentration gradient within the diffusive sublayer
107 (Fig. 1) and steady-state conditions (Garbe et al., 2014). Jørgensen et al. (2020) argued that, due
108 to seawater's high buffer capacity, chemical gradients do not significantly affect CO_2

109 equilibration, supporting the use of measurements at 3-4 m depth. However, this conclusion
110 relies on the assumption of horizontal and vertical homogeneity and neglects the effects of
111 shallow surface stratification, particularly when alkalinity dilution is involved.

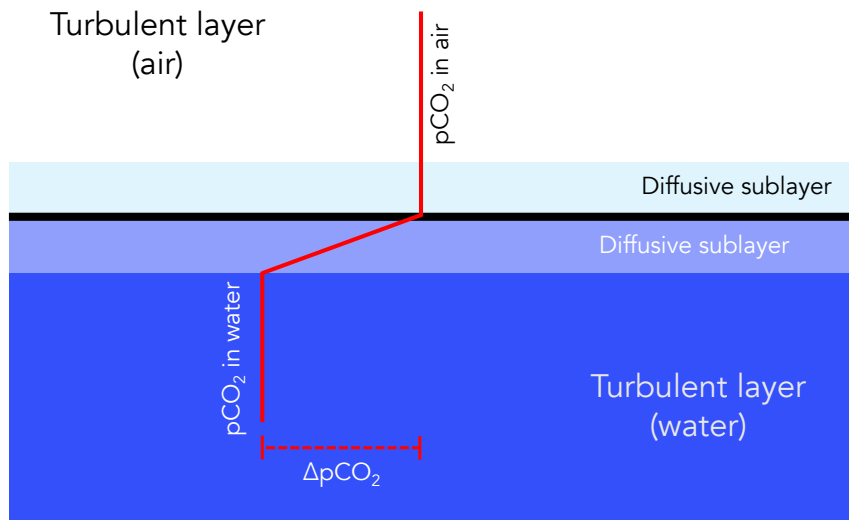
112

113 In Arctic spring, the upper ocean is often strongly stratified due to freshwater input from glacier
114 melt, snowmelt, river runoff, and sea ice meltwater (Ahmed et al., 2020; Granskog et al., 2011;
115 Meire et al., 2017; Miller et al., 2019). These inputs can extend vertical CO₂ gradients beyond
116 the diffusive sublayer, complicating flux estimates during ice breakup and early open-water
117 periods. Several studies have demonstrated strong vertical heterogeneity in pCO₂ in Arctic
118 coastal waters, with implications for air-sea flux calculations (Ahmed et al., 2020; Dong et al.,
119 2021; Miller et al., 2019).

120 Surface freshening from ice melt and runoff strongly influences carbonate chemistry in Arctic
121 coastal waters, which can either suppress or enhance oceanic CO₂ uptake. For example, Burgers
122 et al. (2017) reported large horizontal variability in surface pCO₂ (144–364 μatm) linked to
123 riverine input in the Eastern Canadian Arctic. Similarly, Sejr et al. (2011) observed strong
124 surface pCO₂ gradients associated with salinity and temperature in Young Sound, and later
125 documented a long-term decline in surface salinity (Sejr et al., 2017). Freshwater-induced
126 stratification has also been shown to create vertical gradients in pCO₂ and pH with important
127 implications for flux calculations (Miller et al., 2019). Finally, Bates et al. (2014) demonstrated
128 that sea ice meltwater and melt ponds exhibit extreme variability in pCO₂ (<10 to >1500 μatm)
129 and pH (6.1 to >10.8), highlighting the complex chemical landscape of ice-influenced waters.
130 Together, these studies underscore the high spatial and temporal variability of carbonate
131 chemistry in freshened waters across the Arctic.

132 To project future CO₂ uptake or outgassing in the Arctic, we must better understand the physical
133 and chemical drivers of near-surface carbonate variability. In this study, we investigate the
134 vertical and temporal variations in pCO₂ in a stratified Arctic fjord during sea ice breakup. By
135 examining water-column pCO₂ profiles across the transition from ice-covered to open water, we
136 evaluate usage of the bulk flux model under Arctic seasonal transitions.

137



138
139

140 **Figure 1.** Schematic illustrating the interface between the air and the water in conjunction with
141 pCO₂ concentration gradients. In equation 1, the concentration gradient is assumed to occur in the
142 diffusive layer between the air and water, and the concentrations are assumed to be vertically
143 constant in the turbulent layers. (Adapted from Liss and Slater, 1974; Wanninkhof et al., 2009)

144

145 2. Study Site and Measurement Methods

146

147 2.1 Study Site

148 This study was conducted in Young Sound, a high Arctic fjord system located near the Daneborg
149 Research Station in Northeast Greenland (Fig. 2). The fjord system comprises the Tyrolerfjord
150 (inner fjord) and Young Sound (outer fjord), extending approximately 90 km from Tyroler River
151 to the Greenland Sea. A sill at about 45 m depth separates Young Sound from the open ocean.
152 Young Sound is 2 to 7 km wide, with an average depth of 100 m (maximum 350 m), and a total
153 surface area of ~390 km². Tidal amplitudes range from 0.8 to 1.5 m, with mean current velocities
154 of approximately 2 cm s⁻¹ (Rysgaard et al., 2003). Freshwater inputs are primarily derived from
155 Greenland Ice Sheet runoff, local glaciers, precipitation, and snowmelt from adjacent ice-free
156 terrain. The drainage basin of the Tyrolerfjord-Young Sound system spans 2846 km², of which
157 33% is glaciated.

158

159 Sampling was conducted from 12 to 31 July 2017. Sampling occurred during and immediately
160 after a period of sea ice breakup. On 15 July, ice coverage was approximately 30%, decreasing to
161 less than 10% by 16 July. Water sampling was conducted both from an inflatable boat and via
162 sea ice leads, all in close proximity to the Greenland Ecosystem Monitoring (GEM) program's
163 standard station (Fig. 2).

164

165

166

167 **2.2 pCO₂ Measurements Using the HydroC Sensor**

168 Surface water pCO₂ was measured with a CONTROS® HydroC CO₂ sensor, which utilizes a
169 membrane equilibrator coupled with a non-dispersive infrared detector (Henson et al., 2025b).
170 The instrument is equipped with a built-in water pump that provides flow rate of 35 ml s⁻¹ across
171 the membrane. At each sampling depth, the sensor was allowed to equilibrate for 10 to 20
172 minutes, and values were recorded once stable for at least two minutes. The sensor operates over
173 a range of 200-1000 µatm and temperatures of -2 to 35°C. Annual calibration has been
174 conducted using a certified 400 ± 2% ppm CO₂ gas that was traceable to WMO standards. The
175 sensor showed remarkable stability (397-401 ppm), supporting a measurement uncertainty of ± 2
176 µatm.

177 **2.3 pCO₂ Estimation from TA and DIC**

178 In addition to direct measurements, pCO₂ was calculated from total alkalinity (TA) and dissolved
179 inorganic carbon (DIC) using the Seacarb package (Gattuso et al., 2024) in R. Due to the low
180 salinity and cold temperatures characteristic of Arctic coastal waters, no universally accepted set
181 of equilibrium constants (K1 and K2) exists. For consistency with previous studies in the region
182 of equilibrium constants (K1 and K2) exists. For consistency with previous studies in the region
183 (Henson et al., 2023), we used the refitted constants from (Lueker et al., 2000). The selection of
184 equilibrium constants introduces assumptions regarding seawater composition. (Raimondi et al.,
185 2019) showed that different constants can lead to discrepancies between measured and calculated
186 pCO₂ values, ranging from -3.1 to -35.8 µatm, with Lueker et al. (2000) demonstrating the best
187 internal consistency under polar conditions. Still, (Sulpis et al., 2020) found that the calculation
188 of pCO₂ from DIC and TA can lead to uncertainty up to 15% under cold conditions, which is far
189 greater than when pCO₂ is measured directly.

190 **2.4 Sea Ice TA and DIC Sampling**

191 TA and DIC in sea ice were assessed using three ice cores. Each core was sectioned into 5-10 cm
192 segments and sealed in gas-tight NEN/PE bags with sampling valves (Hansen et al., 2000).
193 Samples were transported in thermally insulated boxes to a nearby field laboratory. Cold (1°C)
194 deionized water of known mass and carbonate composition (10 - 30 ml) was added to each bag,
195 which was then resealed after removing air and weighted.

196
197
198 The samples were melted in the dark over ~48 hours. Meltwater was transferred to 12 mL
199 Exetainer vials (Labco, UK) pre-dosed with 20 µl of saturated HgCl₂ solution (5% w/v) to
200 prevent microbial alteration. DIC was measured by on Apollo SciTech®'s AS-C3 analyzer while
201 TA was determined via potentiometric titration on an Apollo SciTech AS-ALK2 total alkalinity
202 titrator (Haraldsson et al., 1997).

203 **2.5 Physical Parameters**

204 Vertical profiles of conductivity, temperature, and depth (CTD) were obtained using a Seabird®
205 SBE19plus CTD. On 16 July 2017, additional surface conductivity measurements were taken
206

207 using a Thermo Orion-Star® instrument with an Orion 013610MD conductivity cell. Surface
208 water temperatures were independently measured with a Testo® thermometer.

209

210 **2.6 Historical Data**

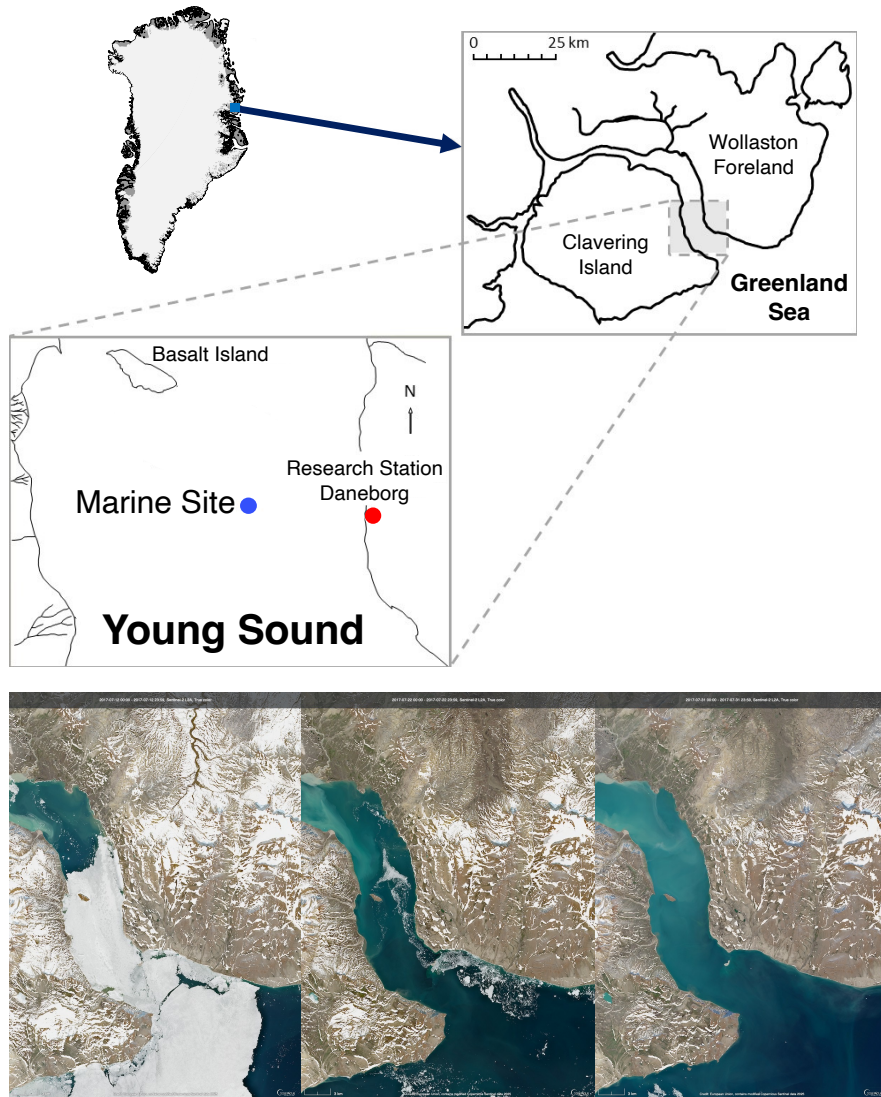
211 For contextual comparison, pCO₂ time series data (Greenland Ecosystem Monitoring, 2020)
212 from the Greenland Ecosystem Monitoring program are also included in the analysis. pCO₂ data
213 from 2007-2023 was measured using the same HydroC CO₂ sensor in August each year.

214

215 **2.7 Eddy Covariance**

216 Sensible and latent heat fluxes were estimated using micrometeorological instrumentation
217 mounted on a 3-meter mast positioned approximately 0.5 meters from the waterline. Three-
218 dimensional wind vectors were recorded using a METEK® uSonic-Scientific sonic anemometer.
219 To enhance reliability, we applied complementary analysis techniques for flux estimation: (1) the
220 standard eddy covariance (EC) method using EddyPro software (Version 7.0.6, LI-COR Inc.,
221 2019); (2) the ogive optimization method (OGM) (Sievers et al., 2015a). Among these, the OGM
222 was deemed most robust due to its ability identify and filter out low-frequency noise, sensor
223 dampening, and large-scale turbulent motions that can bias flux measurements. These issues
224 often introduce large relative bias associated with flux measurement over Arctic marine surfaces
225 (Sievers et al., 2015b). OGM's superior ability to isolate relevant turbulent scales and reduce
226 contamination from mesoscale variability is based on the accumulation and modelling of each
227 cospectra over each 20 min averaging period (Fig. S1 and S2). Uncertainty in sensible and latent
228 heat fluxes was estimated directly from the OGM procedure. The reported values correspond to
229 the standard error associated with the fitted ogive tail and reflect random uncertainty in flux
230 integration.

231



232
233

234 **Figure 2.** Map of Greenland and the sampling area at the coast of Young Sound in Northeast
235 Greenland. The red circle indicates the location of the micrometeorological measurement tower
236 at research station Daneborg while the marine sampling site (Standard Station in the Greenland
237 Ecosystem Monitoring program) is indicated as a blue circle (74.310, -20.300). Three
238 Copernicus Sentinel true-color images of the fjord on July 12, 22, and 31 illustrate the transition
239 between sea ice cover and open water.

240

241 **3 Data and results**

242 Vertical profiles of surface water $p\text{CO}_2$ were measured using the CONTROS® HydroC CO_2
243 sensor across three distinct periods in July 2017 (Fig. 3a-c). Each observational period
244 corresponded to different sea ice conditions: before, during and after sea ice breakup (Fig. 2).
245 These high-resolution profiles revealed substantial vertical variability within the upper 2 to 3
246 meters of the water column. Under ice-covered conditions, $p\text{CO}_2$ measurements were taken

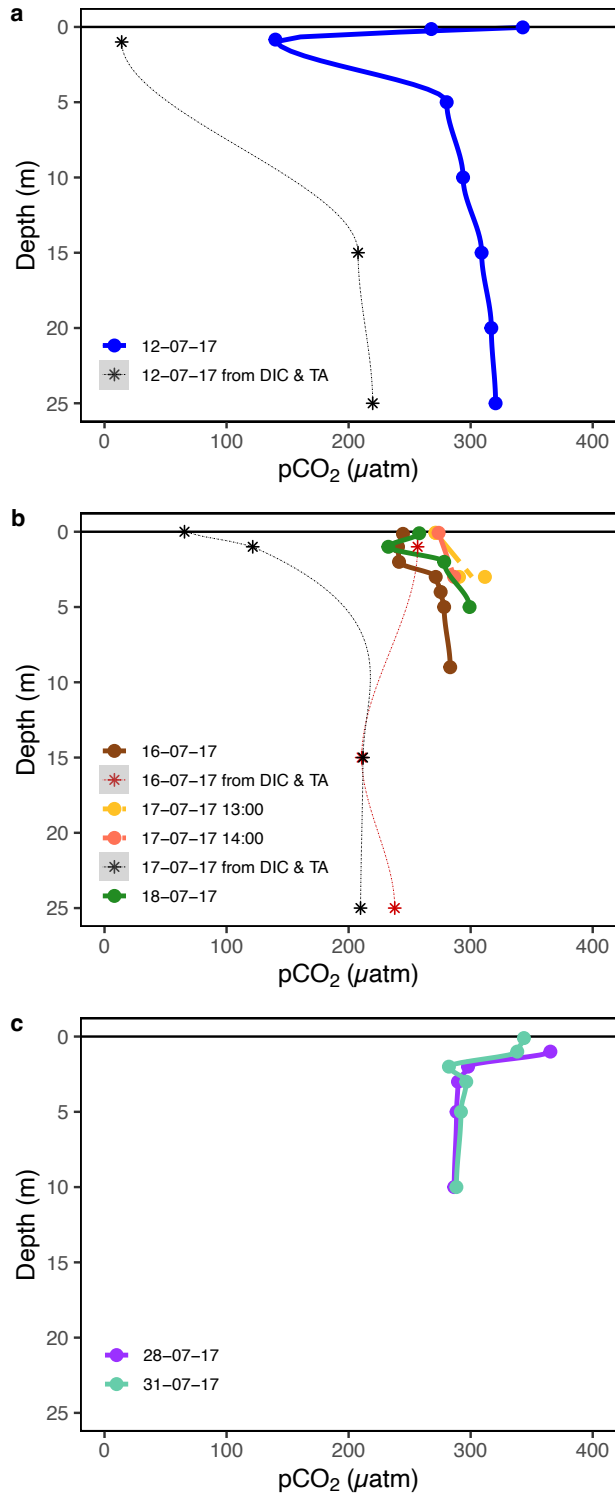
247 through an open melt pond. At this time, elevated CO₂ concentrations were observed at the very
248 surface (0.1 m), followed by a sharp decrease to approximately 1 meter depth, coinciding with
249 the ice-water interface. Below this depth, pCO₂ increased again, though remained well below
250 atmospheric concentrations (Fig. 3a).

251
252 During the period of sea ice breakup, when ice coverage ranged from approximately 30% to
253 10%, the vertical distribution of pCO₂ exhibited a similar structure. Concentrations were highest
254 near the surface, declined to a local minimum at 1 to 2 meters, and then stabilized below 3
255 meters (Fig. 3b). Following the complete breakup of sea ice, pCO₂ showed a more gradual
256 decrease from the surface down to about 3 meters, beneath which concentrations remained
257 relatively constant (Fig. 3c). Across all three observational periods, a shallow surface layer
258 approximately 5 m thick was identified, within which most of the pCO₂ variability occurred.
259 Below this depth, pCO₂ remained relatively constant.

260
261 These vertical structures are consistent with strong physical stratification, likely driven by
262 freshwater input from glacial melt and surface heating. Temperature and salinity profiles
263 collected concurrently support the presence of sharp vertical gradients in the upper water
264 column, with salinity ranging from 1.4 to 29.6 PSU and temperature from -0.4°C to 6.2°C. These
265 physical profiles, shown in Fig. 4, confirm that vertical mixing was strongly suppressed during
266 the observational period. The small tides present in Young Sound, combined with the continued
267 input of freshwater from first sea ice and then glacial melt, lead to a fjord system with distinct
268 surface stratification throughout the months of July and August.

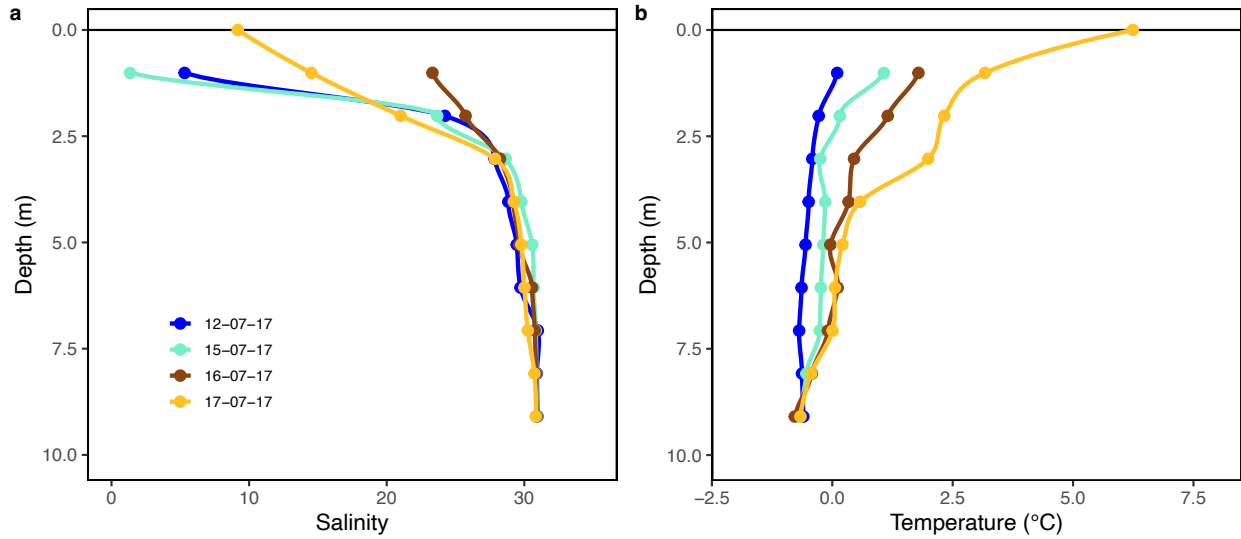
269
270 Measurements from a different fjord (Henson et al., 2025b) in East Greenland on June 4, 2025,
271 revealed strikingly similar vertical pCO₂ heterogeneity (Fig. 5). Elevated pCO₂ at 0.1 m
272 decreased to a minimum around 1-1.5 m before increasing again and stabilizing near 3 m depth.
273 Extreme stratification in the upper few meters caused pCO₂ levels in each profile to vary by
274 more than 100 µatm between the surface and 1 m. This repeated observation of similarly
275 structured nonlinear pCO₂ profiles, measured 8 years later and in a different fjord system,
276 suggests that this heterogeneity is not an isolated phenomenon. Instead, these C-shaped vertical
277 pCO₂ distributions may represent a characteristic response of strongly stratified Arctic surface
278 waters during sea ice breakup. Indeed, Arctic surface stratification during sea ice breakup
279 induces chemical changes that may influence the way we estimate air-sea exchange of CO₂.

280
281
282



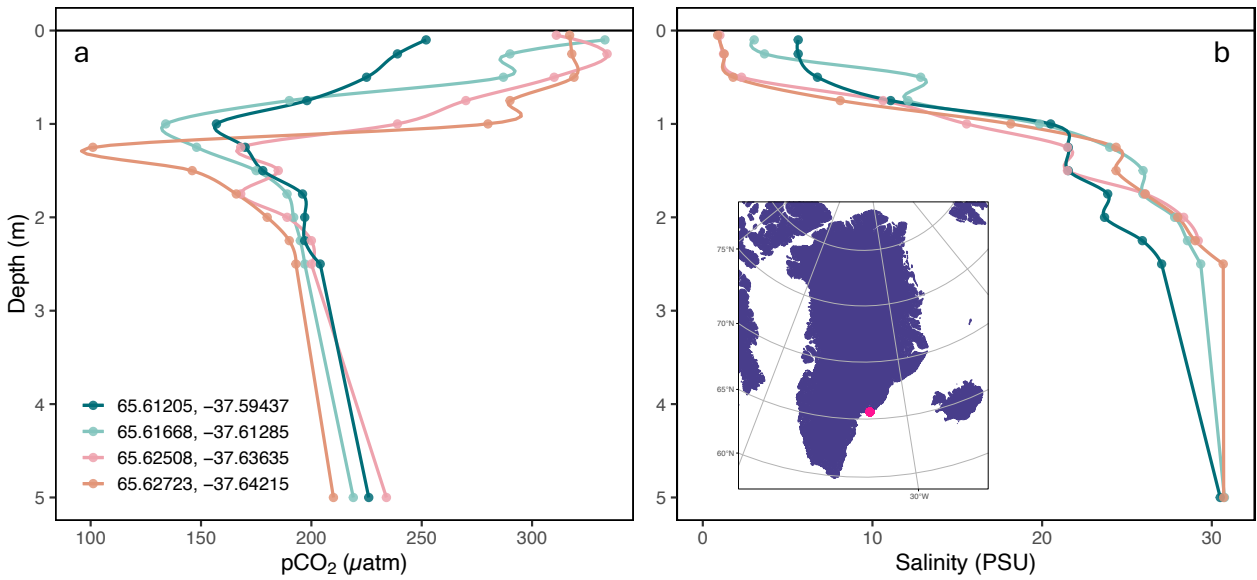
283
 284
 285
 286
 287
 288

Figure 3. Measured Young Sound $p\text{CO}_2$ profiles (a) prior to sea ice breakup (measured through open melt pond), (b) during sea ice breakup and (c) after sea ice break up measured through CO_2 equilibration and calculation from carbonate chemistry parameters (DIC & TA).



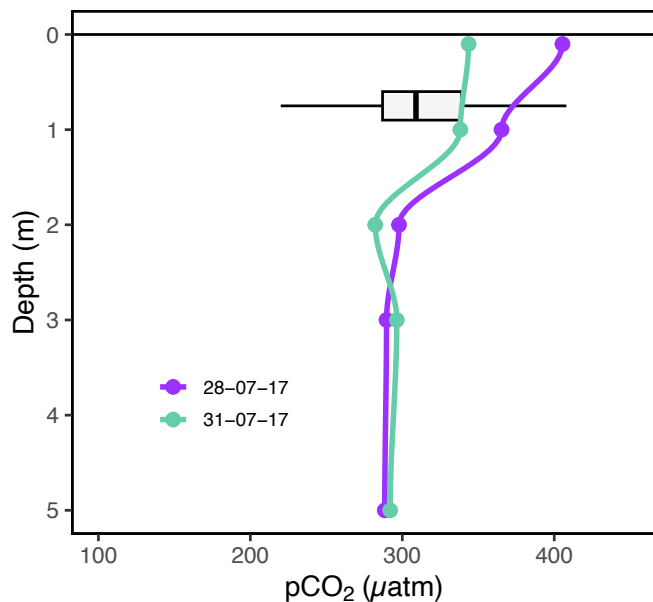
289
290
291
292
293

Figure 4. Measured Young Sound profiles of under-ice water and open water salinity and temperature.



294
295
296
297
298

Figure 5. Measured $p\text{CO}_2$ (a) and salinity (b) profiles at 4 locations in Tasiilaq Bay. Profiles were measured on June 4, 2025 during the period of sea ice breakup following the method in Sejr et al. (2011).



299
300

301 **Figure 6.** Measured Young Sound pCO₂ profile after ice break up in 2017 compared with historical
302 variation in pCO₂ at 1 m depth in the same location.

303
304

305 4. Discussion

306 Air-sea CO₂ fluxes in Arctic coastal areas are generally estimated using bulk parameterization
307 models (Henson et al., 2024; Meire et al., 2015; Roobaert et al., 2019; Sejr et al., 2011). These
308 models rely on several key assumptions, including unstratified surface conditions, a linear pCO₂
309 gradient within the diffusive boundary layer, and a vertically uniform pCO₂ profile within the
310 mixed layer. Our observations challenge the applicability of these assumptions in Arctic coastal
311 waters in several important ways. We observe distinct vertical heterogeneity in both physical and
312 chemical parameters, which leads to distinct differences in flux estimates based on the depth of
313 the measurements used.

314

315 4.1. Stratified conditions in the marine CO₂ system

316 Vertical pCO₂ profiles collected during July 2017 revealed pronounced non-linear behavior in
317 the upper 3 to 5 meters of the water column (Fig. 3). This directly contradicts the assumption that
318 the ΔpCO₂ accurately represents the difference between the atmosphere and the “well-mixed
319 bulk fluid” below the diffusive layer (Wanninkhof et al., 2009). Under ice-covered conditions,
320 the lowest pCO₂ values (~150 ppm) were consistently observed just beneath the sea ice, with
321 concentrations increasing with depth and stabilizing around 5 m (Fig. 3a). During the ice breakup
322 stage, a similar pattern emerged, although the minimum pCO₂ was higher (~250 ppm).

323

324 More recent measurements from Tasiilaq Bay in June 2025 demonstrate very similar vertical
325 pCO₂ profiles. Indeed, 4 high-resolution profiles with measurements every 0.25 m reveal the

326 same C-shaped pCO₂ variation. Like in Young Sound, the most elevated pCO₂ levels were
327 observed near the surface, and pCO₂ minima occurred near 1-2 meters depth before increasing
328 and becoming stable. This repeated observation in a different fjord system, but during the period
329 of sea ice breakup indicates this vertical variability may be representative during stratified Arctic
330 conditions.

331
332 Several interacting processes influence surface water chemistry during ice breakup. Low surface
333 water pCO₂ values reflect the influence of low-salinity meltwater from snow and sea ice or
334 glacial meltwater found in freshened Arctic waters (Geilfus et al., 2015; Henson et al., 2025a).
335 However, surface water chemistry during the ice breakup period is further complicated by
336 processes such as ikaite (CaCO₃·6H₂O) dissolution (Miller et al., 2011; Rysgaard et al., 2013;
337 Søgaard et al., 2013) and high under-ice primary production (Søgaard et al., 2021; Verdugo et
338 al., 2025). Additionally, snowmelt, characterized by low pH and ionic strength (de Caritat et al.,
339 2005), may further alter carbonate system dynamics in the upper water column.

340
341 Two mechanisms may explain the nonlinear C-shaped trend in pCO₂ observed in the top few
342 meters. First, as demonstrated by Henson et al. (2025) mixing between glacial meltwater and
343 seawater can result in nonlinear behavior in pCO₂, even when DIC and TA mix conservatively.
344 In such cases, initial freshwater dilution leads to dramatically reduced pCO₂, but at very low
345 salinities, the diminished buffering capacity can cause acidification to occur and pCO₂ to
346 increase again. In fact, Henson et al. (2025) present a U-shaped pCO₂ curve along a salinity
347 gradient that appears extraordinarily similar to the C-shaped pCO₂ curve we observe with depth.
348 Indeed, the salinity gradient created in their mixing experiments can be observed vertically in the
349 highly stratified surface waters during sea ice breakup (Fig. 3a, 5a). Although, Henson et al.
350 focused on the influence of glacial meltwater, our results suggest similar processes could occur
351 in systems influenced by sea ice and snowmelt.

352
353 Both glacial meltwater and sea ice have low DIC concentrations and act to dilute the inorganic
354 carbon of the surface ocean (Fig. S4). However, changes in alkalinity can also impact the
355 buffering capacity of the water mixture, leading to nonlinear effects. If the meltwater has a lower
356 TA:DIC ratio than seawater, due to the absence of ikaite, acidification and a shift in carbonate
357 equilibria at very low salinities could lead to higher pCO₂ values at the surface. During July
358 2017, Young Sound showed both diluted DIC and TA levels in upper few meters, suggesting pH
359 change during sea ice break up could occur more easily (Fig. S4). Indeed, calculated pH profiles
360 indicated variable surface conditions between periods of sea ice cover and sea ice breakup (Fig.
361 S5). In this very fresh surface layer, diminished pH may elevate pCO₂ relative to waters around 1
362 m depth, where freshwater-seawater mixing ratios are more moderate and seawater buffering
363 leads to very low CO₂ concentrations.

364

365 A second, but less likely, explanation involves atmospheric equilibration of sea ice melt ponds
366 before draining into open leads. The relatively elevated pCO₂ observed at ~0.1 m depth could
367 reflect such partial equilibration. While chamber-based studies (e.g. Geilfus et al., 2012, 2015;
368 Nomura et al., 2010; Semiletov et al., 2004) have demonstrated both uptake and efflux of CO₂ in
369 melt ponds, equilibrium times between melt-pond water and atmosphere depend upon pond
370 depth, wind speed, and carbonate chemistry. For example, a 0.1 m deep pond under low wind
371 conditions (~2 m s⁻¹) may reach atmospheric equilibrium in 1-4 days. However, in our case,
372 pCO₂ values calculated from TA and DIC in melt ponds did not indicate equilibrium with the
373 atmosphere, making this explanation less likely than the freshwater mixing mechanism.
374 Furthermore, Verdugo et al. (2025) demonstrate that melt pond drainage in Young Sound was
375 responsible for reducing pCO₂ levels. Though this conclusion relies on measurements from 2.5
376 m depth. Nevertheless, atmospheric equilibration may play a role after the sea ice barrier is
377 removed. Elevated pCO₂ levels at the surface (0.1 m) post sea ice breakup may result from the
378 combination of the chemical changes described above, heating from solar radiation, and from
379 atmospheric CO₂ uptake (partial equilibration) in the limited volume of this freshwater lens.

380

381 As melt progresses and sea ice recedes, riverine input and vertical mixing become more
382 influential. Yet even after ice breakup, surface waters often remain fresh due to glacial meltwater
383 runoff, and the resulting low salinities help maintain stratification. In August 2017, vertical
384 structure remained pronounced even after sea ice breakup, with elevated pCO₂ at 0.1 m which
385 stabilized below ~3 m. In other words, near-surface conditions remained decoupled from deeper
386 waters. This persistent shallow layer, characterized by low salinity, higher temperature, and
387 elevated pCO₂, suppresses gas exchange with the colder, more undersaturated water below,
388 consistent with observations by Dong et al. (2021). In such environments, bulk flux models that
389 assume homogeneity and linear gradients are likely to yield biased or inaccurate estimates.

390 To place these 2017 measurements in historical context, we examined long-term surface water
391 pCO₂ data collected at 0.5-1 m depth by the Greenland Ecosystem Monitoring (GEM) program
392 between 2007 and 2023. These data, measured using consistent protocols, are presented in Fig. 6
393 alongside our open-water profiles. Over the 17-year record, August pCO₂ concentrations at ~1 m
394 depth had ranged from 220 to 408 μatm and had consistently remained below atmospheric levels.
395 This apparent stability has contributed to the perception of sustained CO₂ uptake throughout the
396 summer season. However, the high-resolution vertical profiles obtained during the 2017 field
397 campaign add nuance to this assumption. Elevated pCO₂ levels confined to the uppermost meter
398 of the water column may go undetected in standard monitoring approaches that rely on fixed-
399 depth sampling. These results suggest that the dynamic changes during sea ice melt can induce
400 episodes of slowed uptake, air-sea equilibrium, or CO₂ outgassing. Consequently, existing
401 sampling protocols may underestimate surface variability and bias flux estimates, especially in
402 stratified conditions where near-surface chemistry is decoupled from subsurface layers.

403

4.2. Influence of surface stratification on fluxes

To assess how bulk models function when estimating CO₂ fluxes in an Arctic fjord influenced by sea ice and snow melt, we calculated fluxes using seawater pCO₂ measurements from multiple depths and two gas transfer velocity parameterizations. Specifically, we computed fluxes throughout July using pCO₂ measured at 0.1, 1, 2, and 4 m. To estimate the surface (interface) pCO₂ at 0 m, we adjusted the 1 m pCO₂ measurements to a derived skin temperature (Table 1), estimated from sensible heat fluxes (Fig. S6) following the parameterization of Smedman et al. (2007). Accounting for this skin layer correction is critical, as Woolf et al. (2016) demonstrated that neglecting the thermal skin and relying only on bulk sea surface temperature can introduce significant errors in flux estimates.

The resulting calculations (Table 1) show that estimated CO₂ fluxes vary significantly depending on the depth of the pCO₂ measurement. Notably, fluxes derived from 0.1 m differ markedly from those based on deeper values. Since many studies rely on pCO₂ measured at a fixed depth (often at 1 m or at a ship's seawater intake below 5 m), these results underscore the potential for misrepresentation of flux magnitude and direction due to vertical heterogeneity in surface water chemistry.

Measurements from both Young Sound and Tasiilaq demonstrate that during sea ice breakup, pCO₂ levels are most elevated at the surface. This may be linked to acidification of the most freshened 0.5 m and a shift in the marine carbonate system, or partial equilibration due to air-sea gas transfer. If this acidified freshwater lens warms, for instance, due to solar radiation, pCO₂ may rise leading to oversaturation relative to atmospheric concentrations. Indeed, when pCO₂ measurements on July 31 were corrected for skin temperature, to estimate pCO₂ at the boundary layer, they suggested a transition from undersaturation to oversaturation (Table 1). While we did not directly observe this oversaturation in the vertical profiles, this likely reflects the inability to sample at the sea surface. Nevertheless, the occurrence of stratification-related vertical pCO₂ heterogeneity, with levels most elevated at the surface, will slow air-sea gas transfer compared to when conditions are well mixed. Meanwhile, warming or acidification of the thin surface layer may periodically induce a reversal of flux direction, as seen in some micrometeorological studies in Arctic coastal environments during sea ice breakup (e.g. Butterworth et al., 2025).

Overall, these findings echo those of Miller et al. (2019), who reported pronounced spatial heterogeneity in Arctic coastal pCO₂ and large differences in estimated fluxes depending on the sampling depth. The broader implications of this heterogeneity for seasonal or regional flux estimates remain unclear. However, if fluxes are upscaled from sparse, single-point measurements (e.g., once per month, as in Laruelle et al., 2014), substantial errors may result due to unrecognized spatial and temporal variability. Thus, our results emphasize the need for continuous, high-resolution observations of air-sea CO₂ fluxes, particularly in Arctic coastal

444 systems affected by stratification and meltwater input. These observations will be essential for
 445 refining flux parameterizations, reducing uncertainty in carbon budget estimates, and improving
 446 the representation of Arctic shelf systems in global carbon models.

447
 448 **Table 1.** CO₂ fluxes calculated based on pCO₂ measured at the different depth. The fluxes are
 449 calculated using the bulk model of Ho et al., 2006 and Nightingale et al. (2000). We have used
 450 locally measured wind speeds for the calculations to match flux measurements captured by eddy
 451 covariance.

452

Date	Depth (m)	Temperature (°C)	Salinity (psu)	pCO ₂ (µatm)	Wind Speed (m s ⁻¹)	Ho (2006)	Nightingale (2000)
						Flux (mmol CO ₂ m ⁻² day ⁻¹)	Flux (mmol CO ₂ m ⁻² day ⁻¹)
16-Jul	0.0	3.0 [†]	23	252 [‡]	6.8	-14.88	-13.69
16-Jul	0.1	3.0	23	244	6.8	-15.78	-14.52
16-Jul	1.0	1.8	26	240	6.8	-16.12	-14.83
16-Jul	2.0	1.1	28	241	6.8	-15.93	-14.66
16-Jul	4.0	0.3	29	275	6.8	-12.19	-11.21
18-Jul	0.0	6.0 [†]	7	262 [‡]	3.3	-3.45	-3.38
18-Jul	0.1	4.3	7	244	3.3	-3.98	-3.90
18-Jul	1.0	3.2	14	233	3.3	-4.20	-4.11
18-Jul	2.0	2.3	21	278	3.3	-2.86	-2.79
18-Jul	4.0	0.6	29	295	3.3	-2.34	-2.29
28-Jul	0.0	10.0 [†]	15	415 [‡]	2.5	0.53	0.54
28-Jul	0.1	10.0	15	405	2.5	0.38	0.38
28-Jul	1.0	7.0	21	365	2.5	-0.22	-0.23
28-Jul	2.0	5.0	27	282	2.5	-1.43	-1.45
28-Jul	4.0	2.0	30	290	2.5	-1.32	-1.34
31-Jul	0.0	12.0 [†]	15	401 [‡]	2.0	0.20	0.21
31-Jul	0.1	10.0	15	343	2.0	-0.36	-0.38
31-Jul	1.0	8.0	21	338	2.0	-0.40	-0.42
31-Jul	2.0	5.0	27	282	2.0	-0.92	-0.97
31-Jul	4.0	2.0	30	294	2.0	-0.81	-0.85

453

454 † Denotes skin temperatures derived from heat fluxes. ‡ Denotes pCO₂ values estimated from
455 measurements at 1 m depth and adjusted to derived skin temperatures.

456
457

458 **5 Conclusions**

459

460 During the summer thaw, carbon chemistry and pCO₂ dynamics in Arctic coastal surface waters
461 are significantly altered by the combined effects of snow and sea ice melt, terrestrial runoff, and
462 biological activity. These influences lead to substantial variability in surface temperature, pH,
463 dissolved inorganic carbon (DIC), and total alkalinity (TA), ultimately disrupting carbonate
464 system equilibrium in the upper water column. As a result, estimating air-sea CO₂ fluxes using
465 traditional bulk models becomes highly uncertain during this period.

466

467 The sea ice breakup period, typically lasting 2-4 weeks, represents a particularly dynamic and
468 complex phase in the annual cycle. Despite its brevity, this phase may have a disproportionate
469 influence on total summer CO₂ uptake, given that open-water conditions in high Arctic fjords are
470 limited to only 80-120 days per year (Sejr et al., 2011).

471

472 Air-sea gas exchange rates depend not only on the pCO₂ gradient between the atmosphere and
473 surface water, but also on rapid, nonlinear changes in surface water chemistry driven by the
474 composition and volume of meltwater and runoff. Accurate flux estimation will therefore require
475 knowledge of the depth at which surface water pCO₂ becomes vertically homogeneous,
476 combined with gas exchange parameterizations tailored to highly stratified and ice-affected
477 conditions. Profiling pCO₂ in the upper water column is therefore essential to identify this depth
478 and to constrain surface flux estimates reliably.

479

480 Several eddy covariance studies in other arctic environments report variable uptake and efflux of
481 CO₂ during the sea ice breakup period (e.g. Butterworth et al., 2025). Building on these findings,
482 our data provides the first step in understanding potential drivers behind this variability. Though,
483 proper quantification of the mechanisms driving nonlinear pCO₂ profiles and the resulting
484 uncertainty of flux estimates will require observations spanning the air-sea boundary. The
485 current lack of these datasets underscores the need for studies that integrate continuous, direct
486 CO₂ flux measurements with detailed observations of surface water carbonate chemistry,
487 atmospheric forcing, skin temperature, and turbulence at the air-ice-water interface.

488

489 Such integrated measurements are critical to improving our understanding of the drivers and net
490 effect of sea ice melt-driven changes on CO₂ fluxes in Arctic coastal systems. Ultimately, this
491 knowledge is essential to accurately quantify the seasonal and regional uptake of atmospheric
492 CO₂ in the rapidly changing Arctic.

493

494

495 **Data Availability**

496 Vertical profiles from both Greenlandic fjords can be found in the Zenodo data repository:
497 <https://doi.org/10.5281/zenodo.17471918>. Long-term data from the Greenland ecosystem
498 monitoring program in Young sound can be accessed at: <https://doi.org/10.17897/A8J4-AF12>.
499

500 **Acknowledgments**

501 This study is a contribution to the GreenFeedback project (Greenhouse gas fluxes and earth
502 system feedbacks, Grant agreement: 101056921), funded by the European Union under the
503 Horizon Europe program, who also supported L.L.S and H.C.H's involvement. H.C.H. was
504 additionally funded by the AUFF (Aarhus Universitets Forskningsfond, project no. AUFF-F-
505 2021-7-7) as part of his PhD. S.R. was funded by Aage V Jensens Fonde (grant no. AVJF21-
506 3012) and the Danish National Research Foundation (grant no. DNRF 185). MKS was funded by
507 the POMP project (Horizon Europe grant: 101136875) and the Connecting the Dots project
508 (Villum Foundation grant: 50110) D.H.S received financial support from the Greenland Climate
509 Research Centre (GCRC), Greenland Institute of Natural Resources. The study also received
510 financial support from The Danish Ministry of Climate, Energy and Utilities, Programme for
511 Arctic Climate, (project: Drivhusgas-observationer i Arktis (ObsArktis), 2017). Furthermore we
512 received support from The Arctic Research Centre, Aarhus University and Greenland Institute of
513 Natural Science. The authors especially wish to thank Egon Randa Frandsen, who assisted with
514 the logistics and the additional measurements in Young Sound. Additionally, the authors would
515 like to recognize the students in the EnCHil Nordic master program, who participated in taking
516 the Tasiilaq measurements. This work is a contribution to the Arctic Science Partnership (ASP)
517 and the MarinBasis component of the Greenland Ecosystem Monitoring Program.
518

519 **Author Contribution**

520 Conceptualization: LLS. Formal analysis, writing – original draft preparation: HCH. Funding
521 acquisition: LLS, SR, MKS, TP. Investigation: DS, BJ, KL, TP, MKS, JS, SR, LLS. Writing –
522 review and editing: DS, TP, MKS, SR, LLS. All the authors have read and agreed to the
523 published version of the paper.
524

525 **Competing interests**

526 The authors declare no competing interests.
527
528

529 **References**

- 530
531 Ahmed, M. M. M., Else, B. G. T., Capelle, D., Miller, L. A., and Papakyriakou, T.: Underestimation of surface *p*
532 CO₂ and air-sea CO₂ fluxes due to freshwater stratification in an Arctic shelf sea, Hudson Bay, *Elementa: Science*
533 *of the Anthropocene*, 8, 084, <https://doi.org/10.1525/elementa.084>, 2020.
- 534 Arrigo, K. R. and van Dijken, G. L.: Continued increases in Arctic Ocean primary production, *Progress in*
535 *Oceanography*, 136, 60–70, <https://doi.org/10.1016/j.pocean.2015.05.002>, 2015.

- 536 Bates, N. R. and Mathis, J. T.: The Arctic Ocean marine carbon cycle: evaluation of air-sea CO₂ exchanges, ocean
537 acidification impacts and potential feedbacks, *Biogeosciences*, 6, 2433–2459, 2009.
- 538 Burgers, T. M., Miller, L. A., Thomas, H., Else, B. G. T., Gosselin, M., and Papakyriakou, T.: Surface Water CO₂
539 Variations and Sea-Air CO₂ Fluxes During Summer in the Eastern Canadian Arctic, *J. Geophys. Res. Oceans*, 122,
540 9663–9678, <https://doi.org/10.1002/2017jc013250>, 2017.
- 541 Butterworth, B. J., Else, B. G. T., Brown, K. A., Mundy, C. J., Williams, W. J., Rotermund, L. M., and de Boer, G.:
542 Annual carbon dioxide flux over seasonal sea ice in the Canadian Arctic, *EGU sphere*, 1–30,
543 <https://doi.org/10.5194/egusphere-2025-1802>, 2025.
- 544 de Caritat, P., Hall, G., Gislason, S., Belsey, W., Braun, M., Goloubeva, N. I., Olsen, H. K., Scheie, J. O., and Vaive,
545 J. E.: Chemical composition of arctic snow: concentration levels and regional distribution of major elements,
546 *Science of The Total Environment*, 336, 183–199, <https://doi.org/10.1016/j.scitotenv.2004.05.031>, 2005.
- 547 Dai, M., Su, J., Zhao, Y., Hofmann, E. E., Cao, Z., Cai, W.-J., Gan, J., Lacroix, F., Laruelle, G. G., Meng, F.,
548 Müller, J. D., Regnier, P. A. G., Wang, G., and Wang, Z.: Carbon Fluxes in the Coastal Ocean: Synthesis, Boundary
549 Processes, and Future Trends, *Annu. Rev. Earth Planet. Sci.*, 50, 593–626, <https://doi.org/10.1146/annurev-earth-032320-090746>, 2022.
- 551 Dong, Y., Yang, M., Bakker, D. C. E., Liss, P. S., Kitidis, V., Brown, I., Chierici, M., Fransson, A., and Bell, T. G.:
552 Near-Surface Stratification Due to Ice Melt Biases Arctic Air-Sea CO₂ Flux Estimates, *Geophysical Research*
553 *Letters*, 48, <https://doi.org/10.1029/2021GL095266>, 2021.
- 554 Garbe, C. S., Rutgersson, A., Boutin, J., de Leeuw, G., Delille, B., Fairall, C. W., Gruber, N., Hare, J., Ho, D. T.,
555 Johnson, M. T., Nightingale, P. D., Pettersson, H., Piskozub, J., Sahlée, E., Tsai, W., Ward, B., Woolf, D. K., and
556 Zappa, C. J.: Transfer Across the Air-Sea Interface, in: *Ocean-Atmosphere Interactions of Gases and Particles*,
557 edited by: Liss, P. S. and Johnson, M. T., Springer, Berlin, Heidelberg, 55–112, https://doi.org/10.1007/978-3-642-25643-1_2, 2014.
- 559 Gattuso, J.-P., Epitalon, J.-M., Lavigne, H., Orr, J., Gentili, B., Hagens, M., Hofmann, A., Mueller, J.-D., Proye, A.,
560 Rae, J., and Soetaert, K.: *seacarb: Seawater Carbonate Chemistry*, 2024.
- 561 Geilfus, N.-X., Carnat, G., Papakyriakou, T., Tison, J.-L., Else, B., Thomas, H., Shadwick, E., and Delille, B.:
562 Dynamics of pCO₂ and related air-ice CO₂ fluxes in the Arctic coastal zone (Amundsen Gulf, Beaufort Sea), *J.*
563 *Geophys. Res.*, 117, n/a-n/a, <https://doi.org/10.1029/2011JC007118>, 2012.
- 564 Geilfus, N.-X., Galley, R. J., Crabeck, O., Papakyriakou, T., Landy, J., Tison, J.-L., and Rysgaard, S.: Inorganic
565 carbon dynamics of melt-pond-covered first-year sea ice in the Canadian Arctic, *Biogeosciences*, 12, 2047–2061,
566 <https://doi.org/10.5194/bg-12-2047-2015>, 2015.
- 567 Granskog, M. A., Kuzyk, Z. Z. A., Azetsu-Scott, K., and Macdonald, R. W.: Distributions of runoff, sea-ice melt
568 and brine using $\delta^{18}\text{O}$ and salinity data — A new view on freshwater cycling in Hudson Bay, *Journal of Marine*
569 *Systems*, 88, 362–374, <https://doi.org/10.1016/j.jmarsys.2011.03.011>, 2011.
- 570 Greenland Ecosystem Monitoring: MarineBasis Zackenberg - Water column - Water pCO₂ (1.0),
571 <https://doi.org/10.17897/A8J4-AF12>, 2020.
- 572 Hansen, J. W., Thamdrup, B., and Jørgensen, B. B.: Anoxic incubation of sediment in gas-tight plastic bags: a
573 method for biogeochemical process studies, *Marine Ecology Progress Series*, 208, 273–282, 2000.
- 574 Haraldsson, C., Anderson, L. G., Hassellöv, M., Hulth, S., and Olsson, K.: Rapid, high-precision potentiometric
575 titration of alkalinity in ocean and sediment pore waters, *Deep Sea Research Part I: Oceanographic Research Papers*,
576 44, 2031–2044, [https://doi.org/10.1016/S0967-0637\(97\)00088-5](https://doi.org/10.1016/S0967-0637(97)00088-5), 1997.

577 Henson, H. C., Holding, J. M., Meire, L., Rysgaard, S., Stedmon, C. A., Stuart-Lee, A., Bendtsen, J., and Sejr, M.:
578 Coastal freshening drives acidification state in Greenland fjords, *Science of The Total Environment*, 855, 158962,
579 <https://doi.org/10.1016/j.scitotenv.2022.158962>, 2023.

580 Henson, H. C., Sejr, M., Meire, L., Sørensen, L. L., Winding, M. H. S., and Holding, J. M.: Resolving Heterogeneity
581 in CO₂ Uptake Potential in the Greenland Coastal Ocean, *Journal of Geophysical Research: Biogeosciences*, 129,
582 e2024JG008246, <https://doi.org/10.1029/2024JG008246>, 2024.

583 Henson, H. C., Puts, I. C., Sejr, M. K., Sørensen, L. L., and Holding, J. M.: Glacial meltwater increases coastal
584 carbon dioxide uptake and sensitivity to biogeochemical change, *Commun Earth Environ*, 6, 687,
585 <https://doi.org/10.1038/s43247-025-02685-4>, 2025a.

586 Henson, H. C., Schröder, D. S., Jensen, B., Lennert, K., Papakyriakou, T., Sejr, M. K., Sievers, J., and Sørensen, L.
587 L.: High-resolution vertical pCO₂ profiles from two Greenlandic fjords during sea-ice breakup,
588 <https://doi.org/10.5281/ZENODO.17471918>, 2025b.

589 Jørgensen, H. E., Sørensen, L. L., and Larsen, S. E.: A Simple Model of Chemistry Effects on the Air-Sea CO₂
590 Exchange Coefficient, *Journal of Geophysical Research: Oceans*, 125, e2018JC014808,
591 <https://doi.org/10.1029/2018JC014808>, 2020.

592 Laruelle, G. G., Lauerwald, R., Pfeil, B., and Regnier, P.: Regionalized global budget of the CO₂ exchange at the
593 air-water interface in continental shelf seas, *Global Biogeochemical Cycles*, 28, 1199–1214,
594 <https://doi.org/10.1002/2014GB004832>, 2014.

595 Liss, P. S. and Slater, P. G.: Flux of Gases across the Air-Sea Interface, *Nature*, 247, 181–184,
596 <https://doi.org/10.1038/247181a0>, 1974.

597 Lueker, T. J., Dickson, A. G., and Keeling, C. D.: Ocean pCO₂ calculated from dissolved inorganic carbon,
598 alkalinity, and equations for K₁ and K₂: validation based on laboratory measurements of CO₂ in gas and seawater at
599 equilibrium, *Marine Chemistry*, 70, 105–119, [https://doi.org/10.1016/s0304-4203\(00\)00022-0](https://doi.org/10.1016/s0304-4203(00)00022-0), 2000.

600 Meire, L., Søgaard, D. H., Mortensen, J., Meysman, F. J. R., Soetaert, K., Arendt, K. E., Juul-Pedersen, T., Blicher,
601 M. E., and Rysgaard, S.: Glacial meltwater and primary production are drivers of strong
602 CO₂ uptake in fjord and coastal waters adjacent to the Greenland Ice Sheet,
603 *Biogeosciences*, 12, 2347–2363, <https://doi.org/10.5194/bg-12-2347-2015>, 2015.

604 Meire, L., Mortensen, J., Meire, P., Juul-Pedersen, T., Sejr, M. K., Rysgaard, S., Nygaard, R., Huybrechts, P., and
605 Meysman, F. J. R.: Marine-terminating glaciers sustain high productivity in Greenland fjords, *Glob Change Biol*, 23,
606 5344–5357, <https://doi.org/10.1111/gcb.13801>, 2017.

607 Miller, L. A., Papakyriakou, T. N., Collins, R. E., Deming, J. W., Ehn, J. K., Macdonald, R. W., Mucci, A., Owens,
608 O., Raudsepp, M., and Sutherland, N.: Carbon dynamics in sea ice: A winter flux time series, *J. Geophys. Res.*, 116,
609 C02028, <https://doi.org/10.1029/2009JC006058>, 2011.

610 Miller, L. A., Burgers, T. M., Burt, W. J., Granskog, M. A., and Papakyriakou, T. N.: Air-Sea CO₂ Flux Estimates
611 in Stratified Arctic Coastal Waters: How Wrong Can We Be?, *Geophys. Res. Lett.*, 46, 235–243,
612 <https://doi.org/10.1029/2018gl080099>, 2019.

613 Nomura, D., Yoshikawa-Inoue, H., Toyota, T., and Shirasawa, K.: Effects of snow, snowmelting and refreezing
614 processes on air–sea-ice CO₂ flux, *Journal of Glaciology*, 56, 262–270,
615 <https://doi.org/10.3189/002214310791968548>, 2010.

616 Perovich, D., Meier, W., Tschudi, M., Hendricks, S., Petty, A. A., Divine, D., Farrell, S., Gerland, S., Haas, C.,
617 Kaleschke, L., Pavlova, O., Ricker, R., Tian-Kunze, X., Webster, M., and Wood, K.: Arctic Report Card 2020: Sea
618 Ice, 2020.

- 619 Raimondi, L., Matthews, J. B. R., Atamanchuk, D., Azetsu-Scott, K., and Wallace, D. W. R.: The internal
620 consistency of the marine carbon dioxide system for high latitude shipboard and *in situ* monitoring, *Marine*
621 *Chemistry*, 213, 49–70, <https://doi.org/10.1016/j.marchem.2019.03.001>, 2019.
- 622 Roobaert, A., Laruelle, G. G., Landschützer, P., Gruber, N., Chou, L., and Regnier, P.: The Spatiotemporal
623 Dynamics of the Sources and Sinks of CO₂ in the Global Coastal Ocean, *Global Biogeochemical Cycles*, 33, 1693–
624 1714, <https://doi.org/10.1029/2019GB006239>, 2019.
- 625 Rysgaard, S., Vang, T., Stjernholm, M., Rasmussen, B., Windelin, A., and Kiilsholm, S.: Physical Conditions,
626 Carbon Transport, and Climate Change Impacts in a Northeast Greenland Fjord, Arctic, Antarctic, and Alpine
627 *Research*, 35, 301–312, [https://doi.org/10.1657/1523-0430\(2003\)035%5B0301:PCCTAC%5D2.0.CO;2](https://doi.org/10.1657/1523-0430(2003)035%5B0301:PCCTAC%5D2.0.CO;2), 2003.
- 628 Rysgaard, S., Søgaard, D. H., Cooper, M., Pu´co, M., Lennert, K., Papakyriakou, T. N., Wang, F.,
629 Geilfus, N. X., Glud, R. N., Ehn, J., McGinnis, D. F., Attard, K., Sievers, J., Deming, J. W., and Barber, D.: Ikaite
630 crystal distribution in winter sea ice and implications for CO₂ system dynamics, *The Cryosphere*, 7, 707–718,
631 <https://doi.org/10.5194/tc-7-707-2013>, 2013.
- 632 Sejr, Krause-Jensen, D., Rysgaard, S., Sørensen, L. L., Christensen, P. B., and Glud, R. N.: Air—sea flux of CO₂ in
633 arctic coastal waters influenced by glacial melt water and sea ice, *Tellus B: Chemical and Physical Meteorology*, 63,
634 815–822, <https://doi.org/10.1111/j.1600-0889.2011.00540.x>, 2011.
- 635 Sejr, M. K., Stedmon, C. A., Bendtsen, J., Abermann, J., Juul-Pedersen, T., Mortensen, J., and Rysgaard, S.:
636 Evidence of local and regional freshening of Northeast Greenland coastal waters, *Sci Rep*, 7, 13183,
637 <https://doi.org/10.1038/s41598-017-10610-9>, 2017.
- 638 Semiletov, I., Makshtas, A., Akasofu, S., and L Andreas, E.: Atmospheric CO₂ balance: The role of Arctic sea ice,
639 *Geophysical Research Letters*, 31, 2003GL017996, <https://doi.org/10.1029/2003GL017996>, 2004.
- 640 Sievers, Papakyriakou, T., Larsen, S. E., Jammet, M. M., Rysgaard, S., Sejr, M., and Sørensen, L. L.: Estimating
641 surface fluxes using eddy covariance and numerical ogive optimization, *Atmospheric Chemistry and Physics*, 15,
642 2081–2103, <https://doi.org/https://doi.org/10.5194/acp-15-2081-2015>, 2015a.
- 643 Sievers, J., Papakyriakou, T., Larsen, S. E., Jammet, M. M., Rysgaard, S., Sejr, M. K., and Sørensen, L. L.:
644 Estimating surface fluxes using eddy covariance and numerical ogive optimization, *Atmospheric Chemistry and*
645 *Physics*, 15, 2081–2103, <https://doi.org/10.5194/acp-15-2081-2015>, 2015b.
- 646 Smedman, A., Högström, U., Sahlée, E., and Cecilia, J.: Critical re-evaluation of the bulk transfer coefficient for
647 sensible heat over the ocean during unstable and neutral conditions, *Quart J Royal Meteorol Soc*, 133, 227–250,
648 <https://doi.org/10.1002/qj.6>, 2007.
- 649 Søgaard, D. H., Thomas, D. N., Rysgaard, S., Glud, R. N., Norman, L., Kaartokallio, H., Juul-Pedersen, T., and
650 Geilfus, N.-X.: The relative contributions of biological and abiotic processes to carbon dynamics in subarctic sea
651 ice, *Polar Biol*, 36, 1761–1777, <https://doi.org/10.1007/s00300-013-1396-3>, 2013.
- 652 Søgaard, D. H., Sorrell, B. K., Sejr, M. K., Andersen, P., Rysgaard, S., Hansen, P. J., Skyttä, A., Lemcke, S., and
653 Lund-Hansen, L. C.: An under-ice bloom of mixotrophic haptophytes in low nutrient and freshwater-influenced
654 Arctic waters, *Sci Rep*, 11, 2915, <https://doi.org/10.1038/s41598-021-82413-y>, 2021.
- 655 Sulpis, O., Lauvset, S. K., and Hagens, M.: Current estimates of K₁* and K₂* appear inconsistent with measured
656 CO₂ system parameters in cold oceanic regions, *Ocean Science*, 16, 847–862, [https://doi.org/10.5194/os-16-847-](https://doi.org/10.5194/os-16-847-2020)
657 2020, 2020.
- 658 Verdugo, J., Ruiz-Castillo, E., Rysgaard, S., Boone, W., Papakyriakou, T., Geilfus, N.-X., and Sørensen, L. L.:
659 Snow and Sea Ice Melt Enhance Under-Ice pCO₂ Undersaturation in Arctic Waters, *Journal of Marine Science and*
660 *Engineering*, 13, 2257, <https://doi.org/10.3390/jmse13122257>, 2025.

- 661 Wanninkhof, R., Asher, W., Ho, D., Sweeney, C., and McGillis, W.: Advances in Quantifying Air-Sea Gas
662 Exchange and Environmental Forcing*, *Annual review of marine science*, 1, 213–44,
663 <https://doi.org/10.1146/annurev.marine.010908.163742>, 2009.
- 664 Watts, J., Bell, T. G., Anderson, K., Butterworth, B. J., Miller, S., Else, B., and Shutler, J.: Impact of sea ice on air-
665 sea CO₂ exchange – A critical review of polar eddy covariance studies, *Progress in Oceanography*, 201, 102741,
666 <https://doi.org/10.1016/j.pocean.2022.102741>, 2022.
- 667 Woolf, D. K., Land, P. E., Shutler, J. D., Goddijn-Murphy, L. M., and Donlon, C. J.: On the calculation of air-sea
668 fluxes of CO₂ in the presence of temperature and salinity gradients, *Journal of Geophysical Research: Oceans*, 121,
669 1229–1248, <https://doi.org/10.1002/2015JC011427>, 2016.
- 670